

# Tractable Approximate Gaussian Inference for Bayesian Neural Networks

James-A. Goulet <sup>\*1</sup> Luong Ha Nguyen <sup>\*1</sup> Saeid Amiri <sup>1</sup>

## Abstract

In this paper, we propose an analytical method allowing for *tractable approximate Gaussian inference* (TAGI) in Bayesian neural networks. The method enables: (1) the analytical inference of the posterior mean vector and diagonal covariance matrix for weights and bias, (2) the end-to-end treatment of uncertainty from the input layer to the output, and (3) the online inference of model parameters using a single observation at a time. The method proposed has a computational complexity of  $\mathcal{O}(n)$  with respect to the number of parameters  $n$ , and the tests performed on regression and classification benchmarks confirm that, for a same network architecture, it matches the performance of existing methods relying on gradient backpropagation.

## 1. Introduction

The estimation of weight and bias in neural networks is currently dominated by approaches employing point estimates when learning model parameters using gradient backpropagation (Rumelhart et al., 1986). Although these approaches allow for the state-of-the-art performance in many domains of applications, it is recognized that they fall short in situations where, for instance, datasets are small, when the task requires quantifying the uncertainty about the prediction made, or for continual learning (Ghahramani, 2015; Kendall & Gal, 2017; Farquhar & Gal, 2019). In such situations, the Bayesian approach for inferring the parameters' posterior probability, is known to be theoretically better suited than a point estimate. This is in theory because applying exact Bayesian inference on large neural networks has been considered to be intractable (Goodfellow et al., 2016).

Many researchers have already proposed approximate inference methods for *Bayesian Neural Networks* (BNN). Early on, it was proposed to employ the *Extended and Unscented Kalman Filter* to estimate the Gaussian posterior for feedforward neural networks (Singhal & Wu, 1989; Puskorius & Feldkamp, 1991; Wan & Merwe, 2000). More recently, this Gaussian framework was extended with the *Cubature filter*

(Arasaratnam & Haykin, 2008), which, like the extended and unscented methods, is limited by the computational complexity of  $\mathcal{O}(n^3)$ , where  $n$  is the number of parameters. In another approach, MacKay (1992) employed the *Laplace approximation* to describe the posterior covariance of parameters. Later, Neal (1995) explored the potential of BNN using *sampling methods*. In parallel, several researchers have applied *variational inference* for estimating the posterior distribution of neural networks' parameters (Hinton & Van Camp, 1993; Barber & Bishop, 1998). The development of moment matching and variational approaches for BNN is still nowadays an active research area (Hernández-Lobato & Adams, 2015; Blundell et al., 2015; Louizos & Welling, 2016; Osawa et al., 2019). Recently, the technique of using Dropout as a Bayesian approximation has received a lot of attention in the community (Gal & Ghahramani, 2016). For all the recent methods that are either based on variational approaches or dropout, the inference of parameters is still treated as an optimization problem relying on gradient backpropagation.

In this paper, we propose a *tractable approximate Gaussian inference* method (TAGI) for Bayesian neural networks. The approach, which does not rely on backpropagation, allows for an analytical end-to-end treatment of uncertainty for the weight and bias parameters, as well as in observed covariates and system responses. The paper is organized as follows: Section 2 first introduces the *Gaussian multiplication approximation* (GMA) for propagating uncertainty in feedforward neural networks, and second, it presents how to perform tractable inference for the posterior mean vector and diagonal covariance of weight and bias parameters. Section 3 validates the performance of the approach on benchmark regression problems and on the MNIST classification problem.

## 2. Gaussian Approximation for BNN

### 2.1. Gaussian Feedforward Neural Network

Figure 1 details the nomenclature for the feedforward neural network (FNN) employed in this paper. Let us consider a vector of input covariates  $\mathbf{X} = [X_1 \ X_2 \ \dots \ X_X]^T : \mathbf{x} \in \mathbb{R}^X$  that are described by random variables in order to take into account errors potentially arising from observation uncertainties, and then suppose we have a vector of  $Y$  observed system responses  $\mathbf{Y} = [Y_1 \ Y_2 \ \dots \ Y_Y]^T : \mathbf{y} \in \mathbb{R}^Y$ . The relations between observed system responses and its covariates are described by the observation model

$$\mathbf{y} = \mathbf{z}^{(0)} + \mathbf{v}, \quad (1)$$

<sup>\*</sup>Equal contribution <sup>1</sup>Dept of Civil Engineering, Polytechnique Montreal, Montreal, Canada. Correspondence to: James-A. Goulet <james.goulet@polymtl.ca>, Luong Ha Nguyen <luong-ha.nguyen@polymtl.ca>.

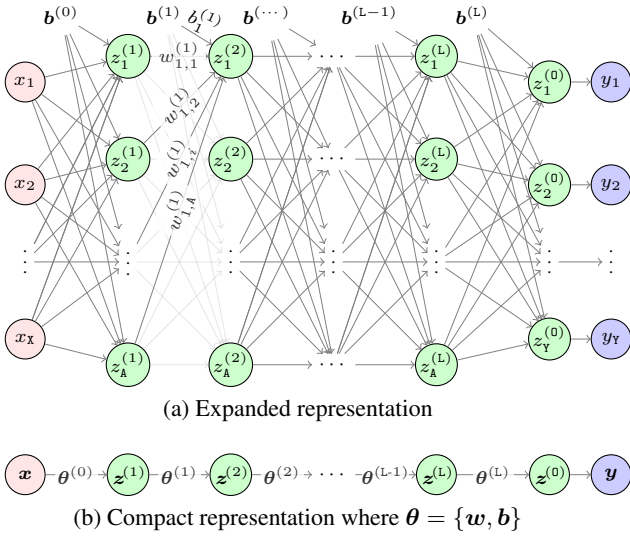


Figure 1. Expanded and compact representations of the variable nomenclature associated with feedforward neural networks.

where the vector of hidden variables  $z^{(0)}$  corresponds to the output layer of a neural network on which observation errors  $\mathbf{v} : \mathbf{V} \sim \mathcal{N}(\mathbf{v}; \mathbf{0}, \Sigma_{\mathbf{V}})$  are added. In common cases,  $\Sigma_{\mathbf{V}}$  is a diagonal covariance matrix assuming that observation errors are independent from each other. We can model the relations between covariates  $\mathbf{x}$  and output hidden variables  $z^{(0)}$  using a feedforward neural network consisting of  $L$  hidden layers each having  $A$  activation units  $a_i^{(j)}$  and hidden variables  $z_i^{(j)}$ ,  $\forall i = \{1, 2, \dots, A\}$ , where an activation unit  $a_i^{(j)}$  is a non-linear transformation of its associated hidden variable,  $a_i^{(j)} = \sigma(z_i^{(j)})$ . We go from the input layer containing the covariates  $\mathbf{x}$ , to the  $i^{\text{th}}$  hidden variable on the first hidden layer, using an affine function of  $\mathbf{x}$  so that

$$z_i^{(1)} = w_{i,1}^{(0)} x_1 + w_{i,2}^{(0)} x_2 + \dots + w_{i,N}^{(0)} x_N + b_i^{(0)}. \quad (2)$$

Equation 2 involves the product of weights  $w_{i,j}^{(0)}$  and covariates  $x_j$  with an additive bias term  $b_i^{(0)}$ . In the context of a neural network, the process of learning consists in estimating these weights and bias. Here we consider that weights and bias parameters are described by random variables so that our joint prior for  $\{\mathbf{X}, \mathbf{W}^{(0)}, \mathbf{B}^{(0)}\}$  is a multivariate Gaussian.

In Equation 2, we note that the product of Gaussian random variables is not Gaussian. Despite this, we propose to employ moment generating functions in order to compute analytically its expected value, its variance, as well as the covariance between the product of Gaussian random variables and any other Gaussian random variable.

For instance, let  $\mathbf{X} = [X_1 \dots X_N]^T \sim \mathcal{N}(\mathbf{x}; \boldsymbol{\mu}, \boldsymbol{\Sigma})$  be a generic vector of Gaussian random variables, where  $\boldsymbol{\mu}$  is the mean vector and  $\boldsymbol{\Sigma}$  is the covariance matrix, then the following

statements are held,

$$\mathbb{E}[X_1 X_2] = \mu_1 \mu_2 + \text{cov}(X_1, X_2), \quad (3)$$

$$\text{cov}(X_3, X_1 X_2) = \text{cov}(X_1, X_3) \mu_2 + \text{cov}(X_2, X_3) \mu_1, \quad (4)$$

$$\text{cov}(X_1 X_2, X_3 X_4) = \text{cov}(X_1, X_3) \text{cov}(X_2, X_4) \quad (5)$$

$$\begin{aligned} &+ \text{cov}(X_1, X_4) \text{cov}(X_2, X_3) \\ &+ \text{cov}(X_1, X_3) \mu_2 \mu_4 + \text{cov}(X_1, X_4) \mu_2 \mu_3 \\ &+ \text{cov}(X_2, X_3) \mu_1 \mu_4 + \text{cov}(X_2, X_4) \mu_1 \mu_3, \end{aligned}$$

$$\begin{aligned} \text{var}(X_1 X_2) = & \sigma_1^2 \sigma_2^2 + \text{cov}(X_1, X_2)^2 \quad (6) \\ & + 2\text{cov}(X_1, X_2) \mu_1 \mu_2 + \sigma_1^2 \mu_2^2 + \sigma_2^2 \mu_1^2. \end{aligned}$$

The development of statements (3-6) is presented in the Appendix A. In this paper, we define the *Gaussian multiplication approximation* as the approximation of the probability density function (PDF) for any product term  $X_i X_j$  by a Gaussian whose first two moments are defined by Equations (3-6). With this approximation, we can now employ  $X_i X_j$  along with the random state vector  $\mathbf{X}$  in affine functions. It allows propagating the uncertainty from the input covariates and prior knowledge on weight and bias parameter through a FNN.

Figure 2a illustrates the passage from the activation units  $\mathbf{A}^{(j)}$ , to a subsequent hidden unit  $Z_i^{(j+1)}$ . Figure 2b-d compare the true theoretical PDF with those obtained using the GMA for different number of activation unit  $A$ , under the assumption that both  $A_k^{(j)} \sim \mathcal{N}(a_k^{(j)}; \mu, \sigma^2)$ ,  $W_{i,k}^{(j)} \sim \mathcal{N}(w_{i,k}^{(j)}; \mu, \sigma^2)$  and  $b_i^{(j)} = 0$ . This shows that even if the GMA is a crude approximation for the Chi-square PDF resulting from the product of two Gaussians, when several of these product terms are added, the result quickly tends to a Gaussian PDF as expected from the central limit theorem.

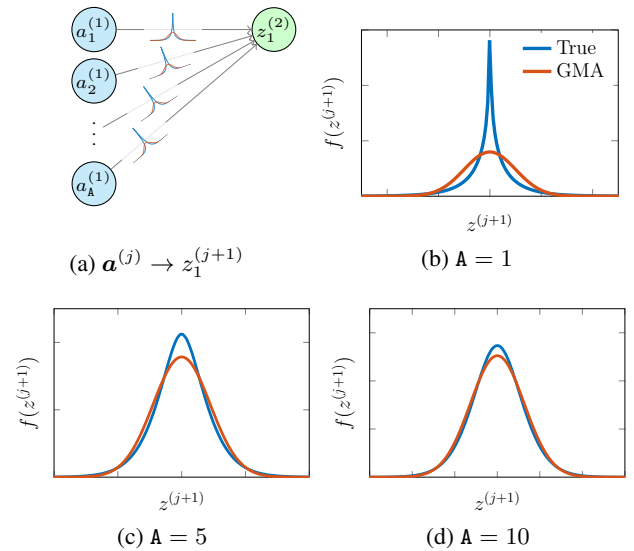


Figure 2. Illustration of the effect of the GMA on the PDF of a hidden unit  $Z_i^{(j+1)}$  as a function of the number of activation units per layer  $A$ . The blue curve represents the true PDF and the red one, the PDF resulting from the GMA approximation.

The passage from the hidden variables  $Z$ , to their correspond-

ing activation units  $\mathbf{A}$  cannot be done analytically using non-linear activation functions. In order to work around this difficulty, we propose to employ functions that are linearized at  $\mathbb{E}[\mathbf{Z}] = \boldsymbol{\mu}_{\mathbf{Z}}$ . *Linearized activation functions*  $\tilde{\sigma}(\cdot)$  allow calculating analytically the expected vector  $\mathbb{E}[\mathbf{A}]$ , the covariance  $\text{cov}(\mathbf{A})$ , as well as the covariance between activation units and the weight and bias  $\text{cov}(\mathbf{A}, \boldsymbol{\theta})$ , where  $\boldsymbol{\theta} = \{\mathbf{W}, \mathbf{B}\}$ . Figure 3 presents an example for the linearization of a softplus activation function. Note that a linearized activation function is not equivalent to having a linear activation function because for each instance of input covariates  $\mathbf{x}_i$ , the linearization is done at a different value  $\mu_z$  which maintains the non-linear dependency between  $\mathbf{x}_i$  and the output  $y_i$ . It is known that this linearization procedure is an approximation of the *change of variable rule* that would be required to obtain true theoretical PDF for  $f(a)$ . It is also known that more advanced sampling-based approaches exist for propagating uncertainty through non-linear function, e.g. (Arasaratnam & Haykin, 2009). Nevertheless, we choose to employ the linearization procedure because of its minimal computational cost which still allows, as it will be shown in §3, to match the state-of-the-art performance on equivalent neural networks architectures using backpropagation. Finally, note that the linearization procedure is compatible with all the common activation functions such as the relu, tanh, logistic sigmoid, etc.

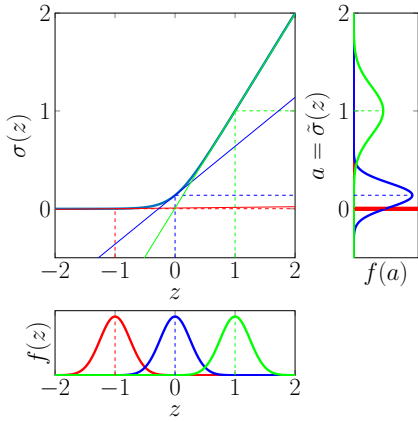


Figure 3. Examples of linearization for a softplus activation function  $\sigma(\cdot)$  at the expected value  $\mathbb{E}[Z]$  for  $Z \sim \mathcal{N}(z; \mu_z, 0.25^2)$  where  $\mu_z = \{-1, 0, 1\}$ .

The transition from the knowledge of the  $j^{\text{th}}$  layer's activation units to an activation unit on the  $j + 1$  layer is defined by  $a_i^{(j+1)} = \tilde{\sigma}(z_i^{(j+1)}) = \tilde{\sigma}(w_{i,1}^{(j)} a_1^{(j)} + w_{i,2}^{(j)} a_2^{(j)} + \dots + w_{i,A}^{(j)} a_A^{(j)} + b_i^{(j)})$ . Analogously, we go from the last hidden layer to the output layer by following

$$z_i^{(0)} = w_{i,1}^{(L)} a_1^{(L)} + w_{i,2}^{(L)} a_2^{(L)} + \dots + w_{i,A}^{(L)} a_A^{(L)} + b_i^{(L)},$$

for all  $i \in \{1, 2, \dots, Y\}$ . All these steps define what we call the *approximate Gaussian feedforward neural network* (AG-FNN), which can be summarized by the input-output relation

$$\{\boldsymbol{\mu}_{\mathbf{Z}}^{(0)}, \boldsymbol{\Sigma}_{\mathbf{Z}}^{(0)}, \boldsymbol{\Sigma}_{\mathbf{Z}\boldsymbol{\theta}}^{(0)}\} = \text{AG-FNN}(\boldsymbol{\mu}_{\mathbf{X}}, \boldsymbol{\Sigma}_{\mathbf{X}}, \boldsymbol{\mu}_{\boldsymbol{\theta}}, \boldsymbol{\Sigma}_{\boldsymbol{\theta}}). \quad (7)$$

For the *regression setup* where  $\mathbf{y} \in \mathbb{R}^Y$ , the observed model output is directly defined by the last layer as described in Equation 1 so that  $\mathcal{N}(\mathbf{y}; \boldsymbol{\mu}_{\mathbf{Y}}, \boldsymbol{\Sigma}_{\mathbf{Y}})$ , where,  $\boldsymbol{\mu}_{\mathbf{Y}} = \boldsymbol{\mu}_{\mathbf{Z}}^{(0)}$ , and  $\boldsymbol{\Sigma}_{\mathbf{Y}} = \boldsymbol{\Sigma}_{\mathbf{Z}}^{(0)} + \boldsymbol{\Sigma}_{\boldsymbol{\theta}}$ .

For the *classification setup*, we need to convert the output  $\mathbf{y} \in \mathbb{R}^Y$  into a class observation  $y^{(c)} \in \{1, 2, \dots, K\}$ , as depicted in Figure 4. Note that using the traditional *Softmax* output

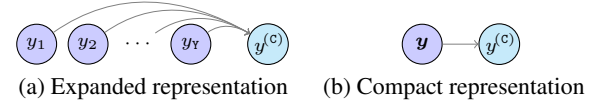


Figure 4. Expanded and compact representations of the output layer for the classification setup.

layer would not allow for a closed-form solution in order to propagate and marginalize the uncertainty associated with the output  $\mathbf{Y}$ . Instead, we propose to employ a *hierarchical binary decomposition* similar to what was employed by Morin & Bengio (2005). For that, each class is encoded in a binary tree with  $H = \lceil \log_2(K) \rceil$  layers, and which is defined by  $Y = K - 1$  hidden states when  $\log_2(K) \in \mathbb{Z}^+$ .

Figure 5 depicts the hierarchical decomposition for  $K = 8$  classes and  $H = 3$  layers, where a given class  $y_C^{(c)} : \mathcal{C} = \{j, k, l\} \in \{0, 1\}^3$  is uniquely described by a set of  $H$  indices. In a binary context where  $H = 1$ , we can transform a regression problem into a probability for a class  $y_i^c$ ,  $i \in \{0, 1\}$  by using

$$p(y_i^c | \mathbf{y}) = \Phi\left((-1)^i \frac{y}{\alpha}\right),$$

where,  $\Phi(\cdot)$  denotes the standard normal CDF, and  $\alpha \in \mathbb{R}^+$  is a scaling factor ensuring the compatibility with the output layer that is intended to return values in the interval  $[-1, 1]$ . In the general case with  $K$ -classes, the conditional probability of a class given the output values  $\mathbf{y}$  is defined by

$$p(y_C^{(c)} | \mathbf{y}) = \prod_{h=1}^H \Phi\left((-1)^{C_h} \frac{[y_C]_h}{\alpha}\right),$$

where  $\mathbf{y}_C = [y_{j0} \ y_{j1} \ y_{jk} \ y_{jk1} \dots]^T \in \mathbb{R}^H$ . For the example in Figure 5 where  $H = 3$  layers, it simplifies to  $\mathbf{y}_C = [y_{j0} \ y_{jk}]^T$ , so that

$$p(y_{\{ijk\}}^{(c)} | \mathbf{y}) = \Phi\left((-1)^i \frac{y_j}{\alpha}\right) \cdot \Phi\left((-1)^j \frac{y_{jk}}{\alpha}\right) \cdot \Phi\left((-1)^k \frac{y_{jk1}}{\alpha}\right).$$

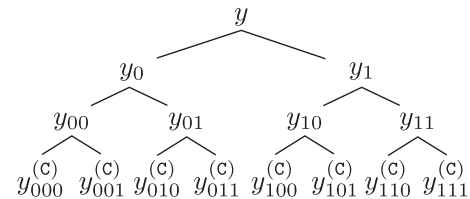


Figure 5. Representation of a 3-layers hierarchical binary decomposition of classes  $y_{ijk}^{(c)} \in \{1, 2, \dots, 8\}$  using the output layer variables  $\mathbf{y} = [y_{j0} \ y_{j1} \ y_{jk} \ y_{jk1} \ y_{jk2}]^T \in \mathbb{R}^7$ .

For the special case where  $\mathbf{Y}_C | \mathcal{D} \sim \mathcal{N}(\mu_{\mathbf{Y}_C}, \text{diag}(\sigma_{\mathbf{Y}_C}^2))$  follows a Gaussian distribution with diagonal covariance, we can employ the development found in [Rasmussen & Williams \(2006\)](#) in order to obtain a closed-form solution to marginalize the output layer's uncertainty,

$$\begin{aligned} p(y_C^{(C)} | \mathcal{D}) &= \int p(y_C^{(C)} | \mathbf{y}_C) \cdot f(\mathbf{y}_C | \mathcal{D}) d\mathbf{y} \\ &= \prod_{h=1}^H \Phi \left( (-1)^{C_h} \frac{[\mu_{\mathbf{Y}_C}]_h}{\sqrt{\alpha^2 + [\sigma_{\mathbf{Y}_C}^2]_h}} \right), \end{aligned} \quad (8)$$

where  $\alpha$  is a scaling factor that enable working with either normalized or unnormalized data. Note that in the case where number of classes  $K$  does not correspond to an integer to the power 2, it is required to normalize the marginal probabilities obtained in Equation 8 in order to account for the unused leaves from the binary tree. During the training phase where we infer the network's parameters from observations  $y^{(C)} \in \{1, 2, \dots, K\}$ , we convert each class into a  $H$ -component vector  $\mathbf{y}_C \in \{-1, 1\}^H$  so that  $[\mathbf{y}_C]_i = (-1)^{C_i}$ .

## 2.2. Linear Algebra for AG-FNN

In this section, we describe how the steps involved in the evaluation of Equation 7 can be performed using linear algebra. Our first hypothesis supposes that the knowledge for covariates, hidden units, as well as the weights and bias, is described by Gaussian random variables. We can then generalize the operations for going from the  $A$  activation units at a layer  $j$  to the subsequent  $A$  hidden units at layer  $j + 1$  using linear algebra so that

$$\underbrace{\begin{bmatrix} Z_1^{(j+1)} \\ Z_2^{(j+1)} \\ \vdots \\ Z_A^{(j+1)} \end{bmatrix}}_{\mathbf{Z}^{(j+1)}} = \underbrace{\begin{bmatrix} W_{1,1}^{(j)} & W_{1,2}^{(j)} & \dots & W_{1,A}^{(j)} \\ W_{2,1}^{(j)} & W_{2,2}^{(j)} & \dots & W_{2,A}^{(j)} \\ \vdots & \vdots & \ddots & \vdots \\ W_{A,1}^{(j)} & W_{A,2}^{(j)} & \dots & W_{A,A}^{(j)} \end{bmatrix}}_{\mathbf{W}^{(j)}} \times \underbrace{\begin{bmatrix} A_1^{(j)} \\ A_2^{(j)} \\ \vdots \\ A_A^{(j)} \end{bmatrix}}_{\mathbf{A}^{(j)}} + \underbrace{\begin{bmatrix} B_1^{(j)} \\ B_2^{(j)} \\ \vdots \\ B_A^{(j)} \end{bmatrix}}_{\mathbf{B}^{(j)}}. \quad (9)$$

Our prior knowledge for activation units is described by  $\mathbf{A}^{(j)} \sim \mathcal{N}(\mathbf{a}^{(j)}; \mu_{\mathbf{A}}^{(j)}, \Sigma_{\mathbf{A}}^{(j)})$  as well as by the covariance  $\text{cov}(\boldsymbol{\theta}, \mathbf{A}^{(j)})$  between the activation units and the vector  $\boldsymbol{\theta} \in \mathbb{R}^P$  containing all the weights and bias parameters defined for all the layers in the network. We can re-write Equation 9 by breaking down the matrix-vector product  $\mathbf{W} \times \mathbf{A}$ , into an operation-wise equivalent vector  $(\mathbf{WA}) \in \mathbb{R}^{A^2 \times 1}$ . We can then employ Equation 3 in order to compute the expected vector  $\mu_{\mathbf{WA}}^{(j)} \equiv \mathbb{E}[(\mathbf{WA})^{(j)}]$ , Equation 5-6 for the covariance matrix  $\Sigma_{\mathbf{WA}}^{(j)} \equiv \text{cov}((\mathbf{WA})^{(j)}) \in \mathbb{R}^{A^2 \times A^2}$  associated with the product terms  $(\mathbf{WA})^{(j)} \in \mathbb{R}^{A^2}$ , and Equation 4 for the covariance matrix  $\Sigma_{\mathbf{WA}\boldsymbol{\theta}}^{(j)} \equiv \text{cov}((\mathbf{WA})^{(j)}, \boldsymbol{\theta}) \in \mathbb{R}^{A^2 \times P}$ . We then introduce two new deterministic matrices  $\mathbf{F}_{wa}^{(j)} \in \{0, 1\}^{A \times A^2}$  and  $\mathbf{F}_b^{(j)} \in \{0, 1\}^{A \times A}$ , which allow rewriting Equation 9 as a system of linear equations involving the product-terms vector  $(\mathbf{WA})$ ,

$$\mathbf{Z}^{(j+1)} = \mathbf{F}_{wa}^{(j)} (\mathbf{WA})^{(j)} + \mathbf{F}_b^{(j)} \mathbf{B}^{(j)}. \quad (10)$$

Note that  $\mathbf{F}_{wa}^{(j)}$  and  $\mathbf{F}_b^{(j)}$  are non-unique as their specific definition depend on the ordering of variables in the problem. An exemple of structure for these matrices is presented in [Appendix B](#). Using the properties of linear functions of Gaussian random variables, we obtain

$$\begin{aligned} \mu_{\mathbf{Z}}^{(j+1)} &\equiv \mathbb{E}[\mathbf{Z}^{(j+1)}] = \mathbf{F}_{wa}^{(j)} \mu_{\mathbf{WA}}^{(j)} + \mathbf{F}_b^{(j)} \mu_{\mathbf{B}}^{(j)}, \\ \Sigma_{\mathbf{Z}}^{(j+1)} &\equiv \text{cov}(\mathbf{Z}^{(j+1)}) = \mathbf{F}_{wa}^{(j)} \Sigma_{\mathbf{WA}}^{(j)} \mathbf{F}_{wa}^{(j)\top} \\ &\quad + \mathbf{F}_b^{(j)} \Sigma_{\mathbf{B}}^{(j)} \mathbf{F}_b^{(j)\top} \\ &\quad + 2 \mathbf{F}_{wa}^{(j)} \text{cov}(\mathbf{WA}^{(j)}, \mathbf{B}^{(j)}) \mathbf{F}_b^{(j)\top}, \\ \Sigma_{\mathbf{Z}\boldsymbol{\theta}}^{(j+1)} &\equiv \text{cov}(\mathbf{Z}^{(j+1)}, \boldsymbol{\theta}) = \mathbf{F}_{wa}^{(j)} \Sigma_{\mathbf{WA}\boldsymbol{\theta}}^{(j)} + \Sigma_{\mathbf{B}\boldsymbol{\theta}}^{(j)}, \end{aligned} \quad (11)$$

where  $\Sigma_{\mathbf{B}\boldsymbol{\theta}}^{(j)} \equiv \text{cov}(\mathbf{B}^{(j)}, \boldsymbol{\theta}) \in \mathbb{R}^{A \times P}$  is the covariance between the bias parameters from the  $j^{\text{th}}$  layer and all the other parameters. In order to apply the linearized activation function  $\mathbf{A}^{(j+1)} = \tilde{\sigma}(\mathbf{Z}^{(j+1)})$ ,

$$\mathbf{A}^{(j+1)} = \mathbf{J}^{(j+1)} \left( \mathbf{Z}^{(j+1)} - \mu_{\mathbf{Z}}^{(j+1)} \right) + \sigma(\mu_{\mathbf{Z}}^{(j+1)}), \quad (12)$$

we need to define the diagonal Jacobian matrix of the transformation evaluated at  $\mu_{\mathbf{Z}}^{(j+1)}, \mathbf{J}^{(j+1)} = \text{diag}(\nabla_{\mathbf{Z}} \sigma(\mu_{\mathbf{Z}}^{(j+1)}))$ . Using again the properties of linear functions of Gaussian random variables, we obtain

$$\begin{aligned} \mu_{\mathbf{A}}^{(j+1)} &\equiv \mathbb{E}[\mathbf{A}^{(j+1)}] = \tilde{\sigma}(\mu_{\mathbf{Z}}^{(j+1)}), \\ \Sigma_{\mathbf{A}}^{(j+1)} &\equiv \text{cov}(\mathbf{A}^{(j+1)}) = \mathbf{J}^{(j+1)} \Sigma_{\mathbf{Z}}^{(j+1)} \mathbf{J}^{(j+1)\top}, \\ \Sigma_{\mathbf{A}\boldsymbol{\theta}}^{(j+1)} &\equiv \text{cov}(\mathbf{A}^{(j+1)}, \boldsymbol{\theta}) = \mathbf{J}^{(j+1)} \Sigma_{\mathbf{Z}\boldsymbol{\theta}}^{(j+1)}. \end{aligned} \quad (13)$$

Equations 11 & 13 allow propagating the information about the covariance of activation units and its dependence on parameters through any pairs of successive layers. For the input layer, the steps described in Equations 9-13 remain the same excepted that the activation units  $\mathbf{A}^{(j)}$  are replaced by the covariates  $\mathbf{X} \sim \mathcal{N}(\mathbf{x}; \mu_{\mathbf{X}}, \Sigma_{\mathbf{X}})$ .

## 2.3. Tractable Approximate Gaussian Inference (TAGI)

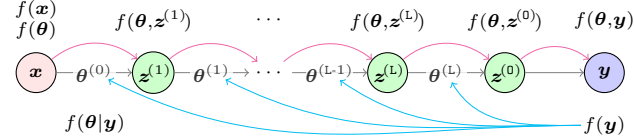
Let us assume we have a set of joint observations for covariates and system responses so that  $\mathcal{D} = \{\mathcal{D}_x, \mathcal{D}_y\} = \{(\mathbf{x}_i, \mathbf{y}_i), \forall i \in \{1 : D\}\}$ . Given that our prior knowledge for the neural network's parameter is  $f(\boldsymbol{\theta}) = \mathcal{N}(\boldsymbol{\theta}; \mu_{\boldsymbol{\theta}}, \Sigma_{\boldsymbol{\theta}})$ , the method presented in [§2.1](#) supposes that the joint PDF  $f(\boldsymbol{\theta}, \mathbf{y})$  for parameters  $\boldsymbol{\theta}$  and observations  $\mathbf{y}$  is Gaussian with mean vector and covariance

$$\boldsymbol{\mu} = \begin{bmatrix} \mu_{\boldsymbol{\theta}} \\ \mu_{\mathbf{Y}} \end{bmatrix}, \quad \Sigma = \begin{bmatrix} \Sigma_{\boldsymbol{\theta}} & \Sigma_{\boldsymbol{\theta}\mathbf{Y}} \\ \Sigma_{\mathbf{Y}\boldsymbol{\theta}} & \Sigma_{\mathbf{Y}} \end{bmatrix}.$$

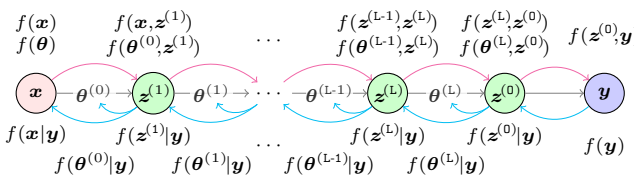
The conditional PDF for the vector  $\boldsymbol{\theta}$  given observations  $\mathbf{Y} = \mathbf{y}$  is described by the Gaussian conditional equations  $f(\boldsymbol{\theta} | \mathbf{y}) = \mathcal{N}(\boldsymbol{\theta}; \mu_{\boldsymbol{\theta}|\mathbf{y}}, \Sigma_{\boldsymbol{\theta}|\mathbf{y}})$  defined by its conditional mean vector and covariance matrix,

$$\begin{aligned} \mu_{\boldsymbol{\theta}|\mathbf{y}} &= \mu_{\boldsymbol{\theta}} + \Sigma_{\boldsymbol{\theta}\mathbf{Y}}^{\top} \Sigma_{\mathbf{Y}}^{-1} (\mathbf{y} - \mu_{\mathbf{Y}}) \\ \Sigma_{\boldsymbol{\theta}|\mathbf{y}} &= \Sigma_{\boldsymbol{\theta}} - \Sigma_{\boldsymbol{\theta}\mathbf{Y}}^{\top} \Sigma_{\mathbf{Y}}^{-1} \Sigma_{\mathbf{Y}\boldsymbol{\theta}}. \end{aligned} \quad (14)$$

This 1-step network-wise inference procedure is computationally prohibitive because the forward propagation of uncertainty depicted in Figure 6a involves large-sized densely populated matrices, and the inference using Equation 14 again involves full matrices.



(a) Intractable 1-step network-wise inference (Eq. 14)



(b) Tractable recursive layer-wise inference (Eq. 15–17)

Figure 6. Representation of the *forward* propagation of uncertainty (magenta arrows) and *inference* procedures (cyan arrows).

The solution we propose to overcome these challenges is twofold: (1) employ a diagonal covariance structure for both the parameters  $\theta$ , and hidden units  $Z^{(j)}$ , and (2) use the inherent conditional independence of hidden units between layers, that is,  $Z^{(j-1)} \perp\!\!\!\perp Z^{(j+1)} | z^{(j)}$ , in order to perform recursive layer-wise inference. As depicted in Figure 6b, the first step consists in inferring the posterior mean vector and diagonal covariance for the output layer following

$$\begin{aligned} f(z^{(0)}|y) &= \mathcal{N}(z^{(0)}; \mu_{Z^{(0)}|y}, \Sigma_{Z^{(0)}|y}) \\ \mu_{Z^{(0)}|y} &= \mu_{Z^{(0)}} + \Sigma_{YZ^{(0)}}^\top \Sigma_Y^{-1} (y - \mu_Y) \\ \Sigma_{Z^{(0)}|y} &= \Sigma_{Z^{(0)}} - \Sigma_{YZ^{(0)}}^\top \Sigma_Y^{-1} \Sigma_{YZ^{(0)}}. \end{aligned} \quad (15)$$

Note that for classification problems, because of the hierarchical formulation described in §2.1, even if there are  $Y$  classes, only  $H = \lceil \log_2(Y) \rceil$  hidden units from the output layer are updated for each observation.

In order to perform layer-wise inference for hidden units and parameters, we define the short-hand notation  $\{\theta^+, Z^+\} \equiv \{\theta^{(j+1)}, Z^{(j+1)}\}$  and  $\{\theta, Z\} \equiv \{\theta^{(j)}, Z^{(j)}\}$ . As depicted in Figure 6b, the inference for the  $j^{\text{th}}$  layer's weights  $\theta$  and hidden units  $Z$  is done using the Rauch-Tung-Striebel recursive procedure (Rauch et al., 1965) where

$$\begin{aligned} f(z|y) &= \mathcal{N}(z; \mu_{Z|y}, \Sigma_{Z|y}) \\ \mu_{Z|y} &= \mu_Z + \mathbf{J}_Z (\mu_{Z^+|y} - \mu_{Z^+}) \\ \Sigma_{Z|y} &= \Sigma_Z + \mathbf{J}_Z (\Sigma_{Z^+|y} - \Sigma_{Z^+}) \mathbf{J}_Z^\top \\ \mathbf{J}_Z &= \Sigma_{ZZ^+} \Sigma_{Z^+}^{-1}, \end{aligned} \quad (16)$$

$$\begin{aligned} f(\theta|y) &= \mathcal{N}(\theta; \mu_{\theta|y}, \Sigma_{\theta|y}) \\ \mu_{\theta|y} &= \mu_\theta + \mathbf{J}_\theta (\mu_{Z^+|y} - \mu_{Z^+}) \\ \Sigma_{\theta|y} &= \Sigma_\theta + \mathbf{J}_\theta (\Sigma_{Z^+|y} - \Sigma_{Z^+}) \mathbf{J}_\theta^\top \\ \mathbf{J}_\theta &= \Sigma_{\theta Z^+} \Sigma_{Z^+}^{-1}. \end{aligned} \quad (17)$$

The key aspect of this approach is that for each layer, we only need to store the mean vectors  $\{\mu_\theta, \mu_Z\}$  and the covariances  $\{\Sigma_\theta, \Sigma_Z, \Sigma_{\theta Z^+}, \Sigma_{Z^+}\}$ , where in addition to the relations already given in §2.2,

$$\Sigma_{ZZ^+} = \mathbf{F}_{wa}^{(j)} \text{cov}(\mathbf{W}\mathbf{A}^{(j)}, \mathbf{Z}^{(j)}) + \mathbf{F}_b^{(j)} \text{cov}(\mathbf{B}^{(j)}, \mathbf{Z}^{(j)}).$$

With a diagonal covariance structure for both  $Z$  and  $\theta$ , the covariance matrices defining each layer contain at most  $A^2 + A$  non-zero terms, i.e., the number of weights ( $A^2$ ) and bias ( $A$ ) per layer; Because of the diagonal structures of covariance matrices, equations 15–17 have a computational complexity  $\mathcal{O}(A^2)$ , which scales linearly with the number of hidden layers  $L$ .

## 2.4. Hyper-parameter estimation

There are typically tens of thousands, if not millions, of parameters in  $\theta$ , for which we typically have little or no prior information for defining the hyper-parameters  $\eta^{(0)} = \{\mu_\theta^{(0)}, \Sigma_\theta^{(0)}\}$ . In the case where we have small datasets, the weakly informative prior combined with limited data will lead to a weakly informative posterior. One solution to go around this difficulty while avoiding overfitting is to learn the model parameters over multiple epochs,  $E > 1$ , using a training  $\mathcal{D}_T$  and validation set  $\mathcal{D}_V$ . Here, we propose to employ the posterior's hyper-parameter values at the  $i^{\text{th}}$  iteration  $\eta^{(i)} = \{\mu_{\theta|D_T}^{(i)}, \Sigma_{\theta|D_T}^{(i)}\}$  and use them as the prior's hyper-parameters at the next iteration  $i + 1$ . This recursive procedure is stopped when the marginal likelihood  $f(\mathcal{D}_{y,v}|\mathcal{D}_{x,v}, \eta^{(i)}) = \mathcal{N}(\mathcal{D}_V; \mu_{y_v|\mathcal{D}_T}^{(i)}, \Sigma_{y_v|\mathcal{D}_T}^{(i)})$  for the validation set  $\mathcal{D}_V$ , has reached its maximal value. This procedure is analogous to the empirical Bayes approach (Efron, 2012) where the prior knowledge's hyper-parameters are learnt through the maximization problem

$$\hat{\eta} = \arg \max_{\eta} \int f(\mathcal{D}_{y,v}|\mathcal{D}_{x,v}, \theta) \cdot f(\theta|\eta) d\theta. \quad (18)$$

Note that unlike in Equation 18 where the maximization is explicit, in our case the maximization is implicitly performed by updating over multiple epochs.

## 3. Experiments

### 3.1. 1D toy problem

We apply TAGI to the 1D regression problem  $y = x^3 + v$ ,  $v : V \sim \mathcal{N}(0, 9)$  taken from (Hernández-Lobato & Adams, 2015), using an AG-FNN having a single hidden layer with 100 units, and a ReLU activation function. The objective of this case study is to showcase how TAGI can be applied on small datasets ( $D = 20$  points), and to compare the results obtained by considering either diagonal or full covariance

matrices. In this example, the inference is performed using one observation at a time, where both the covariates  $x$  and observations  $y$  were normalized in the range  $[-1, 1]$ . The optimal number of epochs is identified from a validation set  $\mathcal{D}_v$  consisting in 20 additional points. The prior covariance for bias is initialized to  $\Sigma_B^0 = 0.01 \cdot \mathbf{I}$ , and for weights  $\Sigma_W^0$ , by multiplying the Xavers's approach (Glorot & Bengio, 2010) by a factor 0.25. The prior mean vector is randomly sampled from  $\mu_\theta^0 \sim \mathcal{N}(\mathbf{0}, \Sigma_\theta^0)$ .

Figure 7 compares the true function employed to generate the data, with the AG-FNN (with diagonal covariances) predictions described by their expected values and  $\pm 3\sigma$  confidence regions. We can see in (a) that the prior predictive obtained before updating with observations ( $E = 0$ ) is weakly informative, and that the posterior predictive obtained after the first epoch (b,  $E = 1$ ) is still a poor approximation of the true function. The log-likelihood reported in (d) for the validation set allows identifying that the optimal number of epochs is  $E = 24$ . The log-likelihood values reported in Figure 7d confirms that employing a training set to identify the number of epoch would not be able to prevent overfitting as depicted in (c).

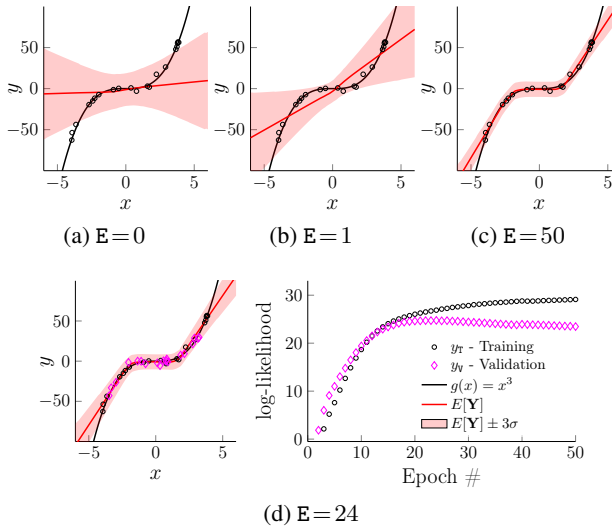


Figure 7. Application of AG-FNN with diagonal covariances to a toy regression problem where (a-c) describe the evolution of the predictive distribution with respect to the number of epochs  $E$ . In (d), we compare the training and validation log-likelihood in order to identify the optimal number of epochs, i.e.,  $E = 24$ .

In a second experiment, we now apply TAGI to the same dataset while considering the full covariance matrices for  $\theta^{(j)}$  and  $z^{(j)}$ . Two networks are studied:  $L=1, A=100$  and  $L=2, A=50$ . Figure 8 displays the sorted correlation coefficients extracted from the upper-triangular posterior covariances, either for each observation from the first epoch, or for the last observation from subsequent epochs. In Figure 8a, for a single hidden layer of 100 units, we can see that the correlation is close to zero for most pairs of parameters and hidden units. In Figure 8b, for a network made of two hidden layers of 50 units, we can see that the correlation is again negligible for most pairs of parameters, and for the hidden units from the

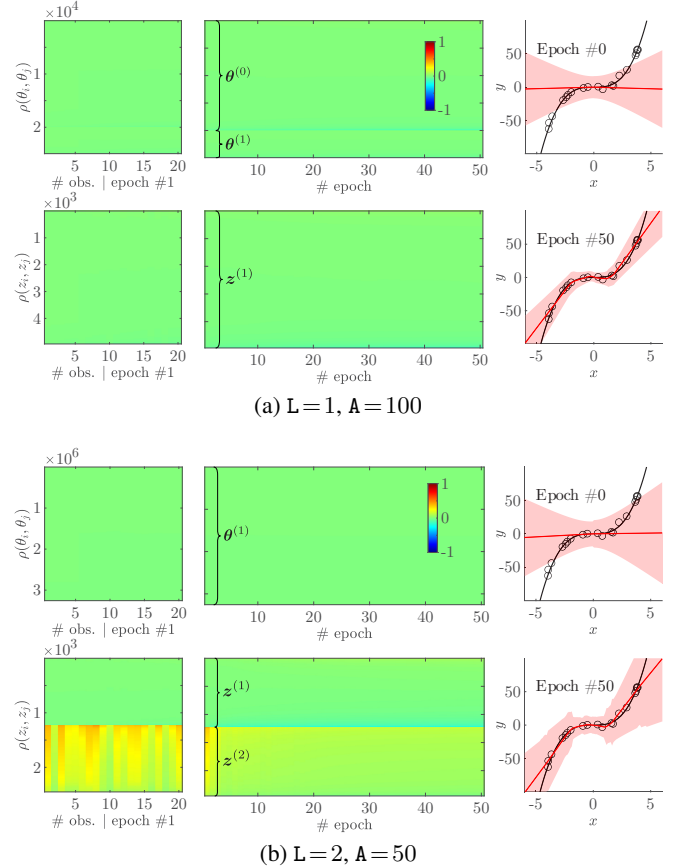


Figure 8. Representation of the sorted correlation coefficients extracted from upper-triangular posterior covariance matrices for the parameters  $\theta^{(j)}$  and hidden units  $z^{(j)}$ . The left-most graphs present the correlations for each of the 20 observations within the first epoch, and the center graphs present the correlations at the end of each epoch.

first layer,  $z^{(1)}$ . For the hidden units on the second layer,  $z^{(2)}$ , the correlation is up to  $\approx 0.5$  during the firsts epochs. This positive correlation on the second hidden layer is caused by the forward propagation of uncertainty from  $z^{(1)} \rightarrow z^{(2)}$ . This positive correlation is not present while going from  $x \rightarrow z^{(1)}$  because here  $x$  is treated as a constant. We can see in Figure 8b that as the number of epochs increases and the parameters' posterior allow capturing the pattern in the data, the positive correlation between the pairs of hidden units in  $z^{(2)}$  vanishes.

These results provide empirical evidence explaining why considering only diagonal covariance matrices may lead to results that are comparable to those obtained while considering the full covariance structure.

### 3.2. Benchmark regression problems

The performance of TAGI is now compared with PBP (Hernández-Lobato & Adams, 2015), VMG (Louizos & Welling, 2016), and MC-dropout (Gal & Ghahramani, 2016) using benchmark regression datasets. For the purpose of comparison with the results from other methods, all the datasets are analyzed for a fixed number of epochs, that is  $E = 40$ .

Table 1. Comparison TAGI's results with PBP (Hernández-Lobato & Adams, 2015), VMG (Louizos & Welling, 2016), and MC-dropout (Gal & Ghahramani, 2016), for E = 40 epochs (Rank legend: **first**, **second**).

Datasets	Root mean square error (RMSE)				Average log-likelihood (LL)			
	PBP	VMG	MC-Dropout	TAGI	PBP	VMG	MC-Dropout	TAGI
Boston	3.01±0.18	<b>2.70±0.13</b>	<b>2.97±0.85</b>	3.02±0.83	<b>-2.56±0.12</b>	<b>-2.46±0.09</b>	<b>-2.46±0.25</b>	<b>-2.56±0.33</b>
Concrete	5.67±0.09	<b>4.89±0.12</b>	<b>5.23±0.53</b>	5.84±0.57	-3.14±0.11	<b>-3.01±0.03</b>	<b>-3.04±0.09</b>	-3.19±0.10
Energy	1.80±0.05	<b>0.54±0.02</b>	1.66±0.19	<b>1.54±0.16</b>	-2.04±0.02	<b>-1.06±0.03</b>	-1.99±0.09	<b>-1.87±0.11</b>
Kin8nm	0.10±0.00	0.10±0.00	0.10±0.00	0.10±4E-3	0.90±0.01	<b>1.10±0.01</b>	<b>0.95±0.03</b>	0.86±0.04
Naval	0.01±0.00	<b>0.00±0.00</b>	0.01±0.00	7E-3±5E-4	<b>3.73±0.01</b>	2.46±0.12	<b>3.80±0.05</b>	3.27±0.20
Power	4.12±0.03	<b>4.04±0.04</b>	<b>4.02±0.18</b>	4.13±0.15	-2.84±0.01	<b>-2.82±0.01</b>	<b>-2.80±0.05</b>	-2.84±0.04
Protein	4.73±0.01	<b>4.13±0.02</b>	<b>4.36±0.04</b>	4.64±0.15	-2.97±0.00	<b>-2.84±0.00</b>	<b>-2.89±0.01</b>	-2.96±6E-3
Wine	0.64±0.01	<b>0.63±0.01</b>	<b>0.62±0.04</b>	<b>0.63±0.04</b>	-0.97±0.01	<b>-0.95±0.01</b>	<b>-0.93±0.06</b>	-0.96±0.06
Yacht	1.02±0.05	<b>0.71±0.05</b>	1.11±0.38	<b>0.86±0.25</b>	-1.63±0.02	<b>-1.30±0.02</b>	<b>-1.55±0.12</b>	<b>-1.30±0.23</b>

For all cases, the data is normalized, the activation function is a ReLU, and the batch size is one, i.e. the inference is performed using one observation at a time; The prior covariance for bias is initialized to  $\Sigma_B^0 = 0.01 \cdot \mathbf{I}$ , and for weights  $\Sigma_W^0$ , by multiplying the Xavers's approach (Glorot & Bengio, 2010) by a factor 0.25; The initial value for the observation error's standard deviation is set to  $\sigma_V = 1$ , and this value is optimized using a 5-fold cross-validation setup.

The results reported in Table 3.1 indicate that TAGI matches the performance of existing methods in term of root mean square error (RMSE) and log-likelihood (LL). Even if VMG displays the best predictive performance, its computational time is two order of magnitude greater than TAGI, PBP and MC-Dropout (Sun et al., 2017). The current TAGI's implementation has a computation time that is comparable to PBP and MC-Dropout (Gal & Ghahramani, 2016). The timing details for each dataset is reported in the Appendix C. Because TAGI had to be implemented from scratch, it is currently not yet fully optimized for computational efficiency. The same is true for the optimization of hyper-parameters such as  $\sigma_V$  which currently rely on a gradient-based approach. Furthermore, the results reported for TAGI did not employ dropout (Srivastava et al., 2014). Also, as it is the case for the other methods reported in Table 3.1, the number of epochs employed was not optimized.

Note as presented in Appendix C, TAGI is not limited to using ReLU and can employ any common activation function. Moreover, the results presented in Appendix C confirm that TAGI is also able to handle deeper architectures, where having more than one hidden layer leads to a performance improvement in 7 out of 9 dataset.

### 3.3. Application on MNIST

We apply TAGI to the MNIST classification problem (LeCun et al., 1998) consisting of  $D = 70\,000$  ( $28 \times 28$ ) greyscale images for  $K = 10$  classes (60 000 training and 10 000 test). Here, we compare the performance of two AG-FNN configurations, each having  $L = 2$  hidden layers with a number of hidden units equal to  $A \in \{100, 800\}$ . Each AG-FNN has the same structure for the input ( $X = 784$  nodes) and the output layer ( $Y = 11$  nodes). The ReLU activation function is used

for the two hidden layers. For each digit, the vector of covariates  $\mathbf{x}_i \in (0, 1)^{784}$  is assumed to be deterministic so that  $\mu_{\mathbf{x}_i} = \mathbf{x}_i$  and  $\Sigma_{\mathbf{x}_i} = \mathbf{0}$ . The prior covariance for bias is initialized to  $\Sigma_B^0 = 0.01 \cdot \mathbf{I}$ , and by using the Xavers's initialization approach (Glorot & Bengio, 2010) for weights  $\Sigma_W^0$ . The prior mean vector is randomly sampled from  $\mu_\theta^0 \sim \mathcal{N}(\mathbf{0}, \Sigma_\theta^0)$ . The hyper-parameter associated with the output layer is set to  $\alpha = 1/3$ . The posterior mean vector as well as the main diagonal of the posterior covariance are learnt using two setups: (1) a single observation per batch, that is,  $B = 1$ , and (2) 10 observations per batch,  $B = 10$ . Each network is evaluated for  $\sigma_V = \{0.1, 0.2, 0.3, 0.4\}$  and the optimal value for  $\sigma_V$  is selected using a randomly selected validation set corresponding to 5% of the training set. The optimal number of epochs  $E$  is identified using an early-stop procedure evaluated on the validation set.

Table 2 presents the average test error evaluated on 10 000 images for the different AG-FNN configurations for  $E = 1$  epoch, and for the optimal number of epochs found using early stop. In order to factor in the effect of random weight initialization, the results reported are the average and standard deviations from five runs. The performance achieved with respect to the average classification errors matches the reported state-of-the-art results of approximately 1.6% for FNNs having a same architecture with 2 layers and 800 hidden units and trained using gradient backpropagation (Simard et al., 2003; Wan et al., 2013). We can see by comparing the results for 100 and 800 hidden units that increasing the hidden layer's size improves the performance both for the first and the optimal number of epochs. Moreover, the results in Table 2 indicate that TAGI's classification accuracy is not significantly affected by the usage of batch sizes greater than one. Nevertheless, we noticed though our experiments that using large batch sizes makes the learning phase sensitive to the network initialization as well as the observation noise parameter  $\sigma_V$ .

We perform a second experiment for an AG-FNN with 2 hidden layers, each having 100 activation units, and where  $\sigma_V = 0.2$ . Figure 9 presents on the leftmost plots, the posterior predictive probability of each class for the test set, where  $D = \{0, 60, 600, 6\,000, 60\,000\}$  observations have been seen during a single epoch,  $E = 1$ . The rightmost plots present

Table 2. MNIST test-set average classification error [%] for the first and last epoch. A: number of hidden units on each layer; B: number of observations per batch; E: number of epochs;  $e$ : optimal number of epoch found using early-stop. The results reported are the average of five runs along with  $\pm$  one standard deviation.

A	B = 1			B = 10				
	E = 1	E = $e$	$e$	$\sigma_V$	E = 1	E = $e$	$e$	$\sigma_V$
100	3.45 $\pm$ 0.19	2.35 $\pm$ 0.12	12 $\pm$ 5	0.2	3.57 $\pm$ 0.09	2.17 $\pm$ 0.10	24 $\pm$ 5	0.4
800	3.21 $\pm$ 0.11	1.51 $\pm$ 0.05	8 $\pm$ 1	0.1	3.26 $\pm$ 0.10	1.53 $\pm$ 0.05	24 $\pm$ 11	0.4

the probability of correct, incorrect, and unknown classes as a function of the threshold classification probability employed  $\phi \in (0.1, 0.999)$ . A *correct class* correspond to the case where the true label has the highest probability among all classes and its probability is  $\geq \phi$ . An *incorrect class* corresponds to the case where an incorrect label has the highest probability among all classes and its probability is  $\geq \phi$ . An *unknown class* correspond to the case where no class has a probability  $\geq \phi$ . Figure 9a-e show a gradual transition from uniform posterior predictive probabilities for  $D=0$  observations, to a low entropy one as  $D$  increases. This confirms that TAGI is suited for online learning whereas it can learn continuously using a single observation at a time and over a single epoch. For reference, Figure 9f shows a how standard neural network relying on backpropagation is unable to learn from a single epoch.

## 4. Conclusion

The tractable approximate Gaussian inference method proposed in this paper allows for: (1) the analytical inference of the posterior mean vector and diagonal covariance matrix for the parameters of Bayesian neural networks, (2) the end-to-end treatment of uncertainty from the input layer to the output layer, and (3) the online Bayesian estimation of model parameters using a single observation at a time. The applications on the regression and classification datasets validate that the approach matches the performance of existing methods with respect to computational efficiency and accuracy. TAGI’s performance and its linear complexity with respect to the number of parameters makes it a viable alternative to gradient backpropagation. By allowing the end-to-end treatment of uncertainty and online inference, we foresee that the approach will enable transformative developments in supervised, unsupervised, and reinforcement learning.

Through our experiments, we noticed that the current architectures and theories developed for backpropagation and employed for defining the network components and initializing its parameters may be sub-optimal for TAGI. Future work in this direction may further improve the performance of the approach.

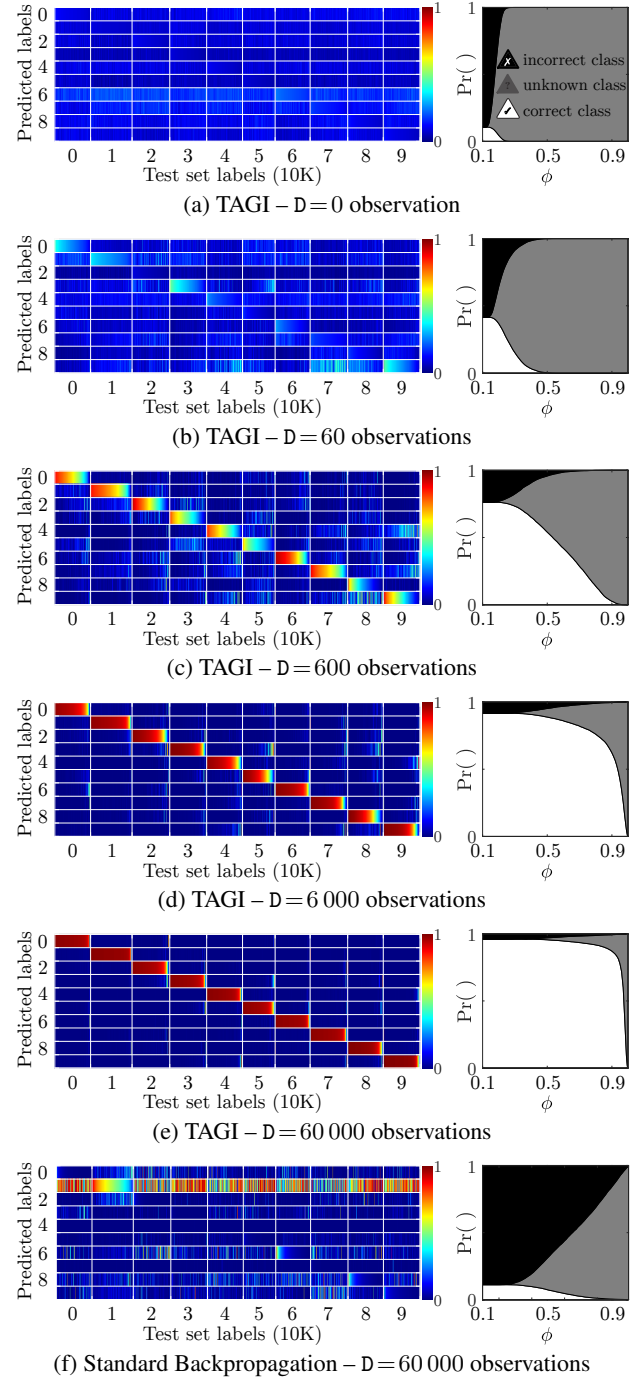


Figure 9. Leftmost graphs describe the posterior predictive probabilities for each class from the test set. The height of each region on rightmost graphs describe the probability of correct (white), incorrect (black), and unknown (gray) classes as a function of the threshold classification probability employed  $\phi \in (0.1, 0.999)$ . All cases are for a single epoch, i.e.,  $E = 1$ .

## Acknowledgements

The second author was financially supported by research grants from Hydro-Quebec, and the Natural Sciences and Engineering Research Council of Canada (NSERC). The third author was supported by a research grant from the Institute for Data Valorization (IVADO).

## References

Arasaratnam, I. and Haykin, S. Nonlinear bayesian filters for training recurrent neural networks. In *Mexican International Conference on Artificial Intelligence*, pp. 12–33. Springer, 2008.

Arasaratnam, I. and Haykin, S. Cubature kalman filters. *IEEE Transactions on automatic control*, 54(6):1254–1269, 2009.

Barber, D. and Bishop, C. M. Ensemble learning in Bayesian neural networks. *NATO ASI Series F Computer and Systems Sciences*, 168:215–238, 1998.

Blundell, C., Cornebise, J., Kavukcuoglu, K., and Wierstra, D. Weight uncertainty in neural network. In *International Conference on Machine Learning*, pp. 1613–1622, 2015.

Efron, B. *Large-scale inference: empirical Bayes methods for estimation, testing, and prediction*, volume 1. Cambridge University Press, 2012.

Farquhar, S. and Gal, Y. A unifying Bayesian view of continual learning. *arXiv preprint arXiv:1902.06494*, 2019.

Gal, Y. and Ghahramani, Z. Dropout as a Bayesian approximation: Representing model uncertainty in deep learning. In *International Conference on Machine Learning*, pp. 1050–1059, 2016.

Ghahramani, Z. Probabilistic machine learning and artificial intelligence. *Nature*, 521(7553):452, 2015.

Glorot, X. and Bengio, Y. Understanding the difficulty of training deep feedforward neural networks. In *Proceedings of the thirteenth International Conference on Artificial Intelligence and Statistics*, pp. 249–256, 2010.

Goodfellow, I., Bengio, Y., and Courville, A. *Deep learning*. MIT Press, 2016.

Hernández-Lobato, J. M. and Adams, R. Probabilistic back-propagation for scalable learning of Bayesian neural networks. In *International Conference on Machine Learning*, pp. 1861–1869, 2015.

Hinton, G. E. and Van Camp, D. Keeping the neural networks simple by minimizing the description length of the weights. In *Proceedings of the sixth annual conference on Computational learning theory*, pp. 5–13. ACM, 1993.

Kendall, A. and Gal, Y. What uncertainties do we need in Bayesian deep learning for computer vision? In *Advances in neural information processing systems*, pp. 5574–5584, 2017.

LeCun, Y., Bottou, L., Bengio, Y., and Haffner, P. Gradient-based learning applied to document recognition. *Proceedings of the IEEE*, 86(11):2278–2324, 1998.

Louizos, C. and Welling, M. Structured and efficient variational deep learning with matrix Gaussian posteriors. In *International Conference on Machine Learning*, pp. 1708–1716, 2016.

MacKay, D. A practical Bayesian framework for backpropagation networks. *Neural computation*, 4(3):448–472, 1992.

Morin, F. and Bengio, Y. Hierarchical probabilistic neural network language model. In *Aistats*, volume 5, pp. 246–252. Citeseer, 2005.

Neal, R. M. *Bayesian learning for neural networks*. PhD thesis, University of Toronto, 1995.

Osawa, K., Swaroop, S., Jain, A., Eschenhagen, R., Turner, R. E., Yokota, R., and Khan, M. E. Practical deep learning with bayesian principles. In *Advances in Neural Information Processing Systems*, 2019.

Puskorius, G. V. and Feldkamp, L. A. Decoupled extended kalman filter training of feedforward layered networks. In *IJCNN-91-Seattle International Joint Conference on Neural Networks*, volume 1, pp. 771–777. IEEE, 1991.

Rasmussen, C. E. and Williams, C. K. *Gaussian processes for machine learning*. the MIT Press, 2006.

Rauch, H. E., Striebel, C. T., and Tung, F. Maximum likelihood estimates of linear dynamic systems. *AIAA journal*, 3(8):1445–1450, 1965.

Rumelhart, D. E., Hinton, G. E., and Williams, R. J. Learning representations by back-propagating errors. *nature*, 323(6088):533, 1986.

Simard, P. Y., Steinkraus, D., and Platt, J. C. Best practices for convolutional neural networks applied to visual document analysis. In *Proceedings of Seventh International Conference on Document Analysis and Recognition*, 2003.

Singhal, S. and Wu, L. Training multilayer perceptrons with the extended kalman algorithm. In Touretzky, D. S. (ed.), *Advances in Neural Information Processing Systems 1*, pp. 133–140. Morgan-Kaufmann, 1989.

Srivastava, N., Hinton, G., Krizhevsky, A., Sutskever, I., and Salakhutdinov, R. Dropout: a simple way to prevent neural networks from overfitting. *The journal of machine learning research*, 15(1):1929–1958, 2014.

Sun, S., Chen, C., and Carin, L. Learning structured weight uncertainty in bayesian neural networks. In *Artificial Intelligence and Statistics*, pp. 1283–1292, 2017.

Wan, E. A. and Merwe, R. v. d. The unscented Kalman filter for nonlinear estimation. In *Adaptive Systems for Signal Processing, Communications, and Control Symposium*, pp. 153–158. IEEE, 2000.

Wan, L., Zeiler, M., Zhang, S., Cun, Y. L., and Fergus, R. Regularization of neural networks using dropconnect. In *Proceedings of the 30th International Conference on Machine Learning*, volume 28 of *Proceedings of Machine Learning Research*, pp. 1058–1066, 2013.

## Appendix

### A. Derivation of moments for the Gaussian multiplicative approximation

The proof of statement (3) can be obtained directly from the definition of covariance. To prove the statement (4), one needs the moments of variables and their products. Because the underlying distribution is Gaussian and its moment generating function is known,  $M_{\mathbf{X}}(\mathbf{t}^\top) = \mathbb{E}[e^{\mathbf{t}^\top \mathbf{X}}] = e^{\mathbf{t}^\top \boldsymbol{\mu} + \frac{1}{2} \mathbf{t}^\top \boldsymbol{\Sigma} \mathbf{t}}$ ,  $\mathbf{t} = [t_1 \dots t_4]^\top$ , all moments can be extracted using the moment-generating function. Using the derivatives of the moment-generating function,

$$\begin{aligned} \mathbb{E}[X_1 X_2 X_3] &= \frac{\partial^3}{\partial t_1 \partial t_2 \partial t_3} \mathbb{E}[e^{\mathbf{t}^\top \mathbf{X}}] \Big|_{t_1=t_2=t_3=t_4=0} \\ &= \frac{\partial^3}{\partial t_1 \partial t_2 \partial t_3} e^{\mathbf{t}^\top \boldsymbol{\mu} + \frac{1}{2} \mathbf{t}^\top \boldsymbol{\Sigma} \mathbf{t}} \Big|_{t_1=t_2=t_3=t_4=0} \\ &= \frac{\partial^3}{\partial t_1 \partial t_2 \partial t_3} e^{\sum_{i=1}^4 t_i \mu_i + \frac{1}{2} \sum_{i,j=1}^4 t_i t_j \text{cov}(X_i, X_j)} \Big|_{t_{1,2,3,4}=0} \\ &= \text{cov}(X_1, X_2) \mu_3 + \text{cov}(X_1, X_3) \mu_2 \\ &\quad + \text{cov}(X_2, X_3) \mu_1 + \mu_1 \mu_2 \mu_3. \end{aligned} \quad (19)$$

Using the definition of covariance and substituting (19), the statement (4) can be established:

$$\begin{aligned} \text{cov}(X_3, X_1 X_2) &= \mathbb{E}[X_1 X_2 X_3] - \mathbb{E}(X_1 X_3) \mathbb{E}(X_2) \\ &= \text{cov}(X_1, X_2) \mu_3 + \text{cov}(X_1, X_3) \mu_2 \\ &\quad + \text{cov}(X_2, X_3) \mu_1 + \mu_1 \mu_2 \mu_3 \\ &\quad - \mu_3 (\mu_1 \mu_2 + \text{cov}(X_1, X_2)). \end{aligned} \quad (20)$$

The expansion of the right side for the last statement leads to Equation (5) so that

$$\text{cov}(X_1 X_2, X_3 X_4) = \mathbb{E}[X_1 X_2 X_3 X_4] - \mathbb{E}[X_1 X_2] \mathbb{E}[X_3 X_4],$$

where the expected value of the product two random variables is given in (3) and the expectation for the product of four random variables is a generalization of (19) that can be obtained using the derivatives of the moment-generating function:

$$\begin{aligned} \mathbb{E}[X_1 X_2 X_3 X_4] &= \frac{\partial^4}{\partial t_1 \partial t_2 \partial t_3 \partial t_4} \mathbb{E}[e^{\mathbf{t}^\top \mathbf{X}}] \Big|_{t_{1,2,3,4}=0} \\ &= \frac{\partial^4}{\partial t_1 \partial t_2 \partial t_3 \partial t_4} e^{\mathbf{t}^\top \boldsymbol{\mu} + \frac{1}{2} \mathbf{t}^\top \boldsymbol{\Sigma} \mathbf{t}} \Big|_{t_{1,2,3,4}=0} \\ &= \text{cov}(X_1 X_2) (\text{cov}(X_3, X_4) + \mu_3 \mu_4) \\ &\quad + \text{cov}(X_1 X_3) (\text{cov}(X_2, X_4) + \mu_2 \mu_4) \\ &\quad + \text{cov}(X_2 X_3) (\text{cov}(X_1, X_4) \\ &\quad + \mu_1 \mu_4) + \text{cov}(X_1, X_4) \mu_2 \mu_3 + \text{cov}(X_2, X_4) \mu_1 \mu_3 \\ &\quad + \text{cov}(X_3, X_4) \mu_1 \mu_2 + \mu_1 \mu_2 \mu_3 \mu_4. \end{aligned}$$

Using the definition of variance

$$\text{var}(X_1 X_2) = \mathbb{E}[(X_1 X_2)^2] - \mathbb{E}[X_1 X_2]^2 \quad (21)$$

The elements of variance can be expended as below

$$\begin{aligned} \mathbb{E}[(X_1 X_2)^2] &= \frac{\partial^4}{\partial t_1^2 \partial t_2^2} \mathbb{E}[e^{\mathbf{t}^\top \mathbf{X}}] \Big|_{t_1=t_2=t_3=t_4=0} \\ &= \frac{\partial^4}{\partial t_1^2 \partial t_2^2} e^{\mathbf{t}^\top \boldsymbol{\mu} + \frac{1}{2} \mathbf{t}^\top \boldsymbol{\Sigma} \mathbf{t}} \Big|_{t_1=t_2=t_3=t_4=0} \\ &= \sigma_1^2 \sigma_2^2 + 2\text{cov}(X_1, X_2)^2 \\ &\quad + 4\text{cov}(X_1, X_2) \mu_1 \mu_2 \\ &\quad + \sigma_1^2 \mu_2^2 + \sigma_2^2 \mu_1^2 + \mu_1^2 \mu_2^2. \end{aligned} \quad (22)$$

$$\begin{aligned} \mathbb{E}[X_1 X_2]^2 &= (\text{cov}(X_1, X_2) + \mathbb{E}(X_1) \mathbb{E}(X_2))^2 \\ &= \text{cov}(X_1, X_2)^2 + 2\text{cov}(X_1, X_2) \mu_1 \mu_2 \\ &\quad + \mu_1^2 \mu_2^2. \end{aligned} \quad (23)$$

Substituting (22) and (23) in (21) establishes (6).

### B. Example of $\mathbf{F}_{wa}^{(j)}$ and in $\mathbf{F}_b^{(j)}$ matrices

Figure 10 presents an example of two successive hidden layers each comprising only two hidden units. The formulation of the

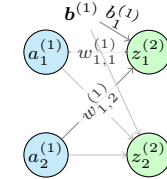


Figure 10. Example of trivial network configuration employed to illustrate the configuration for the matrices  $\mathbf{F}_{wa}^{(j)}$  and  $\mathbf{F}_b^{(j)}$ .

the  $\mathbf{F}_{wa}^{(j)}$  and in  $\mathbf{F}_b^{(j)}$  matrices corresponding to the network in Figure 10 is

$$\begin{bmatrix} z_1^{(2)} \\ z_2^{(2)} \end{bmatrix} = \underbrace{\begin{bmatrix} 1 & 1 & 0 & 0 \\ 0 & 0 & 1 & 1 \end{bmatrix}}_{\mathbf{F}_{wa}^{(j)}} \times \underbrace{\begin{bmatrix} w_{1,1}^{(1)} a_1^{(1)} \\ w_{1,2}^{(1)} a_2^{(1)} \\ w_{2,1}^{(1)} a_1^{(1)} \\ w_{2,2}^{(1)} a_2^{(1)} \end{bmatrix}}_{(\mathbf{u}a)^{(j)}} + \underbrace{\begin{bmatrix} 1 & 0 \\ 0 & 1 \end{bmatrix}}_{\mathbf{F}_b^{(j)}} \times \underbrace{\begin{bmatrix} b_1^{(1)} \\ b_2^{(1)} \end{bmatrix}}_{\mathbf{b}^{(j)}}.$$

Note that the structure of  $\mathbf{F}_{wa}^{(j)}$  depends on the ordering of variables.

### C. Experiment configurations for benchmark regression datasets

Table 3 presents the details for the experiments conducted for the benchmark regression datasets. Note that the times presented in the last columns are the average parameter (i.e. weights and bias) inference time in second per folds and the average hyper parameter (i.e.  $\sigma_V$ ) optimization time in second. All these experiments were conducted using CPU.

Table 3. Experiment details for the benchmark regression datasets using BLNN. X: number of covariates, L: number of layers, A: number of activation units per layer, F number of random training/test folds.

Datasets	Train		Test		Average inference ( $\theta$ )		Average optimization ( $\sigma_V$ )		Average $\sigma_V$ (20 folds)
	X	#obs.	#obs.	$L \times A$	F	time per fold (s)	time per fold (s)		
Boston	13	455	51	1×50	20	4	14		0.32
Concrete	8	927	103	1×50	20	8	22		0.33
Energy	8	691	77	1×50	20	6	24		0.15
Kin8nm	8	7373	819	1×50	20	61	167		0.35
Naval	16	11934	1193	1×50	20	90	280		0.31
Power	4	8611	957	1×50	20	53	124		0.24
Protein	9	41157	4373	1×100	5	363	466		0.72
Wine	11	1439	160	1×50	20	12	20		0.75
Yacht	6	277	31	1×50	20	2	23		0.063

Table 4. Regression benchmark results using the ReLU activation function and different number of hidden layer.

Datasets	Number of hidden layers			
	1	2	3	4
Root mean square error (RMSE)				
Boston	3.02±0.83	2.67±0.73	2.75±0.7	2.78±0.66
Concrete	5.84±0.57	5.10±0.45	5.06±0.54	5.16±0.47
Energy	1.54±0.16	0.50±0.08	0.50±0.07	0.52±0.08
Kin8nm	0.10±4E-3	0.07±3E-3	0.07±1E-3	0.07±2E-3
Naval	7E-3±5E-4	1.4E-3±2E-5	6.5E-4±7E-5	5.2E-4±6E-5
Power	4.13±0.15	3.97±0.16	3.88±0.16	3.85±0.18
Protein	4.64±0.15	4.09±0.01	3.76±0.02	3.65±0.04
Wine	0.63±0.04	0.63±0.04	0.64±0.04	0.64±0.04
Yacht	0.86±0.25	0.70±0.36	0.74±0.29	4.46±6.56
Average log-likelihood (LL)				
Boston	-2.56±0.33	-2.43±0.20	-2.44±0.18	-2.46±0.19
Concrete	-3.19±0.10	-3.06±0.07	-3.06±0.08	-3.07±0.07
Energy	-1.87±0.11	-1.44±0.02	-1.45±0.02	-1.45±0.02
Kin8nm	0.86±0.04	1.16±0.02	1.20±0.01	1.19±0.02
Naval	3.27±0.20	4.42±0.01	4.46±3E-3	4.46±2E-3
Power	-2.84±0.04	-2.80±0.04	2.78±0.04	-2.77±0.04
Protein	-2.96±6E-3	-2.83±0.00	2.78±0.00	-2.75±0.00
Wine	-0.96±0.06	-0.96±0.07	-0.97±0.06	-0.97±0.07
Yacht	-1.30±0.23	-1.19±0.21	-1.27±0.16	-34.65±60.77

Table 5. Regression benchmark results using the softplus activation function and different number of hidden layer.

Datasets	Number of hidden layers			
	1	2	3	4
Root mean square error (RMSE)				
Boston	3.08±0.80	2.84±0.70	2.91±0.60	2.99±0.62
Concrete	5.89±0.47	5.21±0.50	5.31±0.49	5.16±0.47
Energy	1.78±0.25	0.52±0.07	0.52±0.07	0.61±0.13
Kin8nm	0.10±3E-3	0.07±3E-3	0.08±3E-3	0.1±4E-3
Naval	6E-3±3E-4	9E-4±1E-4	5.4E-4±1E-4	4.6E-4±7E-5
Power	4.20±0.15	4.04±0.16	3.99±0.16	3.94±0.18
Protein	4.69±0.03	4.18±0.05	3.84±0.01	3.79±0.02
Wine	0.63±0.03	0.63±0.05	0.65±0.05	0.65±0.05
Yacht	0.98±0.27	1.14±1.02	2.63±1.80	3.85±1.69
Average log-likelihood (LL)				
Boston	-2.56±0.28	-2.45±0.17	-2.48±0.17	-2.52±0.20
Concrete	-3.20±0.09	-3.08±0.08	-3.09±0.08	-3.07±0.07
Energy	-2.05±0.19	-1.43±0.02	-1.44±0.02	-1.45±0.03
Kin8nm	0.88±0.03	1.14±0.02	1.08±0.03	0.88±0.05
Naval	3.70±0.09	4.45±7E-3	4.46±3E-3	4.46±2E-3
Power	-2.85±0.04	-2.82±0.04	-2.80±0.04	-2.79±0.04
Protein	-2.97±7E-3	-2.85±0.01	-2.78±3E-3	-2.77±4E-3
Wine	-0.97±0.06	-0.96±0.07	-1.00±0.08	-1.00±0.08
Yacht	-1.42±0.26	-1.78±1.34	-3.9±4.6	-6.55±0.70